catalysts

MDPI

Article

Alternative Aqueous Phase Synthesis of a PtRu/C Electrocatalyst for Direct Methanol Fuel Cells

Qijun Wang [1], Ya-Wei Zhou [1], Zhao Jin [2,*], Chunguang Chen [1,3], Hong Li [1,*] and Wen-Bin Cai [1,*]

[1] Collaborative Innovation Center of Chemistry for Energy Materials, Shanghai Key Laboratory of Molecular Catalysis and Innovative Materials, Department of Chemistry, Fudan University, Shanghai 200438, China; qjwang17@fudan.edu.cn (Q.W.); zhouyw16@fudan.edu.cn (Y.-W.Z.); cgchen19@usst.edu.cn (C.C.)
[2] State Key Laboratory of Electroanalytical Chemistry, Changchun Institute of Applied Chemistry, Chinese Academy of Sciences, Changchun 130022, Jilin, China
[3] Department of Chemistry, University of Shanghai for Science and Technology, Shanghai 200093, China
* Correspondence: zjin@ciac.ac.cn (Z.J.); hongli17@fudan.edu.cn (H.L.); wbcai@fudan.edu.cn (W.-B.C.); Tel.: +86-431-85262225 (Z.J.); +86-21-31244050 (H.L.); +86-21-31244050 (W.-B.C.)

Abstract: Carbon-supported PtRu nanoalloy (PtRu/C) is widely used as the anode catalyst for direct methanol fuel cells (DMFC), and an aqueous phase synthesis of PtRu/C is in high demand due to for energy-saving and environmentally-benign considerations, however, it is very challenging to attain stoichiometric reduction, good dispersion and a high alloying degree. Herein, we report a facile aqueous phase approach with dimethylamine borane (DMAB) as the reducing agent to synthesize a PtRu/C(DMAB). TEM, XRD, XPS and ICP-AES characterizations indicate that the structural parameters in the PtRu/C(DMAB) are improved significantly as compared to those obtained in a PtRu/C($NaBH_4$) and a commercial PtRu/C, contributing to an enhanced electrocatalytic performance. It turns out that the PtRu/C(DMAB) exhibits the highest methanol electro-oxidation (MOR) performance among all of the tested samples, with the peak current up to 1.8 times as much as that of the state-of-the-art commercial PtRu/C, corroborating the highest output power density in comparative DMFC tests. In-situ attenuated total reflection infrared (ATR-IR) spectroscopy correlates the higher methanol electro-oxidation performance of the PtRu/C(DMAB) with its enhanced CO resistance and CO_2 generation. This simple aqueous synthetic approach may provide an alternative route for developing efficient anode electrocatalysts of DMFCs.

Keywords: PtRu/C catalyst; methanol electro-oxidation reaction; aqueous phase synthesis; dimethylamine borane; direct methanol fuel cell; in-situ ATR-IR

Citation: Wang, Q.; Zhou, Y.-W.; Jin, Z.; Chen, C.; Li, H.; Cai, W.-B. Alternative Aqueous Phase Synthesis of a PtRu/C Electrocatalyst for Direct Methanol Fuel Cells. *Catalysts* **2021**, *11*, 925. https://doi.org/10.3390/catal11080925

Academic Editors: Sabrina Campagna Zignani, José Joaquín Linares León, Ali Seifitokaldani and Bruno Fabre

Received: 23 June 2021
Accepted: 27 July 2021
Published: 30 July 2021

1. Introduction

Direct methanol fuel cells (DMFC) are promising energy-converter to drive portable devices owing to their high efficiency, low emissions and rich fuel supply [1]. Platinum is the primary catalytic metal required for electrocatalytic methanol oxidation in acidic media [2–4]. However, the low abundance and poor CO tolerance of Pt calls for its alloying with a secondary metal in practice [5,6]. Among the Pt-based bimetallic catalysts, carbon supported PtRu (atomic ratio of Pt:Ru = 1:1) alloy nanoparticles (PtRu/C) serve as one type of the most practical anode catalysts for DMFC [7]. The high performance of PtRu/C in methanol electro-oxidation reactions (MOR) has been attributed mainly to the so-called bifunctional mechanism [8] together with the electronic effect [9]. For a total 6-electron oxidation reaction, the main pathway on a Pt-Ru alloy may include [7]:

$$\mathrm{Pt} + \mathrm{CH_3OH} \rightarrow \mathrm{Pt\text{-}CO_{ads}} + 4\mathrm{H^+} + 4\mathrm{e^-} \quad (1)$$

$$\mathrm{Ru} + \mathrm{H_2O} \rightarrow \mathrm{Ru\text{-}OH_{ads}} + \mathrm{H^+} + \mathrm{e^-} \quad (2)$$

$$\mathrm{Pt\text{-}CO_{ads}} + \mathrm{Ru\text{-}OH_{ads}} \rightarrow \mathrm{CO_2} + \mathrm{Pt} + \mathrm{Ru} + \mathrm{H^+} + \mathrm{e^-} \quad (3)$$

In the bifunctional mechanism, Pt favors the dehydrogenation to form CO species while Ru favors the dissociative adsorption of H_2O to form OH_{ad} species at lower potentials, thereby promoting the MOR to CO_2 [10]. Besides, the electronic effect of Ru weakens the CO-adsorption on Pt via lattice shrinkage and partial electron transfer, in favor of oxidative CO removal [11,12].

So far, PtRu/C catalysts have been synthesized by several processes, including impreganation-H_2 reduction [13–16], polyol reduction [17,18], microemulsion [19–22], nano-capsule [23], spray pyrolysis [24,25] and aqueous phase synthesis [26–29]. The non-aqueous phase processes are commonly complicated, environment-unfriendly and cost-ineffective for scaled-up fabrication.

In contrast, the aqueous phase synthesis in which water serves as the solvent for the precursors, complexing agents and reductants without introducing strong surfactants may overcome the above problems, and thus is highly demanded. However, the most challenging issue for this synthetic process is to maintain highly-dispersed and finely-sized Pt-Ru nanoparticles on carbon supports with a desired Pt/Ru atomic ratio and alloying degree. $NaBH_4$ is the most widely-used strong reductant for this synthetic process [26–28], yet the above-mentioned structural aspect and thus the performance of a PtRu/C($NaBH_4$) catalyst are to be improved. HCOOH was tested as the reductant in the aqueous phase synthesis, however, due to its weak reducing power, Ru(III) was under-reduced in the resulting PtRu/C catalysts [29]. Dimethylamine borane (DMAB, $(CH_3)_2NH{\cdot}BH_3$), a water soluble small molecule with a milder but sufficiently strong reducing power [30], was initially developed in our group for the synthesis of a series of carbon supported catalysts such as Pd-B/C [31], Pt-B/C [32], Pt_3Ni-B/C [32] and Pt_3Co/C catalysts [33]. Nevertheless, it is unknown whether the DMAB-derived PtRu/C(DMAB) yields better structure and performance towards MOR than the $NaBH_4$-derived PtRu/C($NaBH_4$).

In this work, we initially extend the DMAB-based aqueous phase process to obtain the PtRu/C(DMAB) with a smaller size, narrower distribution and relatively higher alloying degree. The PtRu/C(DMAB) is characterized by a variety of physicochemical tools, and is assessed for MOR by conventional electrochemical measurements as well as a DMFC test, taking the PtRu/C($NaBH_4$), commercial Pt/C and PtRu/C for comparison. In-situ attenuated total reflection infrared (ATR-IR) spectroscopy is applied to monitor the interfacial species on the catalyst surfaces during MOR to provide a molecular-level understanding of different performances.

2. Results and Discussion

2.1. Synthesis Mechanism of PtRu/C(DMAB) Nanoparticles

DMAB is initially used in this work as the reductant to synthesis of a PtRu/C catalyst. It is noted that the pH plays a crucial role in the synthetic process of the PtRu/C(DMAB). On one hand, the metallic precursor solution containing Ru(III) and Pt(II) species is maintained as acidic to avoid their hydrolysis [29,34]. On the other hand, DMAB is very unstable in acidic media, leading to a significantly decreased reducing power, thus DMAB is better used in a mild alkaline solution. For a balanced consideration in this work, a reverse addition mode is introduced in the reduction process, that is, the acidic metallic precursor solution is added dropwise to the DMAB-contained carbon black slurry of a weak alkalinity. By these means, the nominal reduction of Pt(II) and Ru(III) species at the desired stoichiometric ratio of 1:1 can be obtained.

Equations (4)–(6) show that the reaction mechanism between DMAB and Pt(II)/Ru(III) is analogous to our previous reported work [31]. Firstly, DMAB reacts with OH^- to form BH_3OH^-, and BH_3OH^- is to be the reducing agent. Next, it is possible for each BH_3OH^- to provide six electrons to reduce three Pt(II) or two Ru(III) ions, leading to the formation of PtRu/C(DMAB).

$$(CH_3)_2NH{\cdot}BH_3 + OH^- \rightarrow (CH_3)_2NH + BH_3OH^- \quad (4)$$

$$BH_3OH^- + 3Pt(II) + 2H_2O \rightarrow 3Pt + B(OH_3) + 5H^+ \quad (5)$$

$$BH_3OH^- + 2Ru(III) + 2H_2O \rightarrow 2Ru + B(OH_3) + 5H^+ \quad (6)$$

2.2. Physicochemical Characterization

The compositions of the as-synthesized PtRu/C were determined by ICP-AES analysis of metal nanoparticles dissolved in aqua regia. As listed in Table 1, the atomic percentages of B in the PtRu/C(DMAB) and PtRu/C($NaBH_4$) are negligible (<1.5 at.%). The weight percentages of Pt in PtRu/C(DMAB) and PtRu/C($NaBH_4$) prepared by the reverse addition are 19.0 wt.% and 19.2 wt.% while those of Ru are 10.2 wt.% and 9.9 wt.%, respectively. For the reverse addition mode, the Pt(II) and Ru(III)-contained precursor solution was acidic before reacting with the reductants, which may suppress the hydrolysis of the Ru(III) precursor. Moreover, an excessive amount of the reductant was added into the carbon black slurry with a mild alkalinity beforehand. As a result, the reverse addition aqueous phase synthesis led to the nominal reduction of Pt(II) and Ru(III) species at the desired stoichiometric ratio of 1:1. In the case of the regular addition mode, the determined weight percentages of Pt in PtRu/C(DMAB) and PtRu/C($NaBH_4$) were 18.5 wt.% and 20.0 wt.% while those of Ru were 7.0 wt.% and 6.8 wt.%, respectively. The incomplete reduction of Ru(III) precursor may be chiefly due to the hydrolysis of the Ru(III) precursor [29,34]. In the following sections, only the PtRu/C(DMAB) and PtRu/C($NaBH_4$) catalysts prepared by the reverse addition are investigated.

Table 1. The ICP-AES results of PtRu/C(DMAB) and PtRu/C($NaBH_4$) prepared by the reverse addition and regular addition, respectively.

Catalysts	Adding Mode	Pt (wt.%)	Ru (wt.%)	B (at.%)	Pt/Ru Ratio of Charge	Pt/Ru Atomic Ratio
PtRu/C(DMAB)	reverse addition	19.0	10.2	1.27	1.0:1	1.0:1
PtRu/C($NaBH_4$)		19.2	9.9	0.90		1.0:1
PtRu/C(DMAB)	regular addition	18.5	7.0	1.32		1.4:1
PtRu/C($NaBH_4$)		20.0	6.8	0.88		1.5:1

Figure 1 presents the typical TEM images of Johnson Matthey (JM) Pt/C, JM PtRu/C, PtRu/C(DMAB) and PtRu/C($NaBH_4$) catalysts. The statistically mean sizes of metallic nanoparticles for JM Pt/C and JM PtRu/C are 2.7 $\pm$ 0.5 nm and 2.6 $\pm$ 0.4 nm, respectively. For comparison, PtRu/C(DMAB) and PtRu/C($NaBH_4$) show mean PtRu particle sizes of 2.0 $\pm$ 0.2 nm and 2.7 $\pm$ 0.4 nm, respectively. The larger size and poorer dispersion of PtRu nanoparticles on carbon black in PtRu/C($NaBH_4$) may arise from the stronger reducing power of $NaBH_4$, showing the advantage of the milder reductant DMAB.

XRD patterns of JM Pt/C, JM PtRu/C, PtRu/C(DMAB) and PtRu/C($NaBH_4$) catalysts are shown in Figure 2. The XRD pattern of JM Pt/C exhibits (111), (200) and (220) diffraction peaks at 2θ values of 39.8°, 46.2°, 67.4°, respectively (black dashed lines, PDF#04-0802), indicating a Pt face-centered cubic (fcc) structure [35]. Separated Ru peaks are absent in all PtRu/C catalysts (red dashed lines, PDF#06-0663), which suggest that they are mainly in an alloy phase. The (111) diffraction peaks of the PtRu/C catalysts are shifted positively compared to those of JM Pt/C, in agreement with lattice shrinkage in a PtRu alloy [11]. The resulting Pt d-band downshift of the PtRu alloy is expected to contribute partly to its increased resistance to CO poisoning, in addition to the well-known bifunctional mechanism [12].

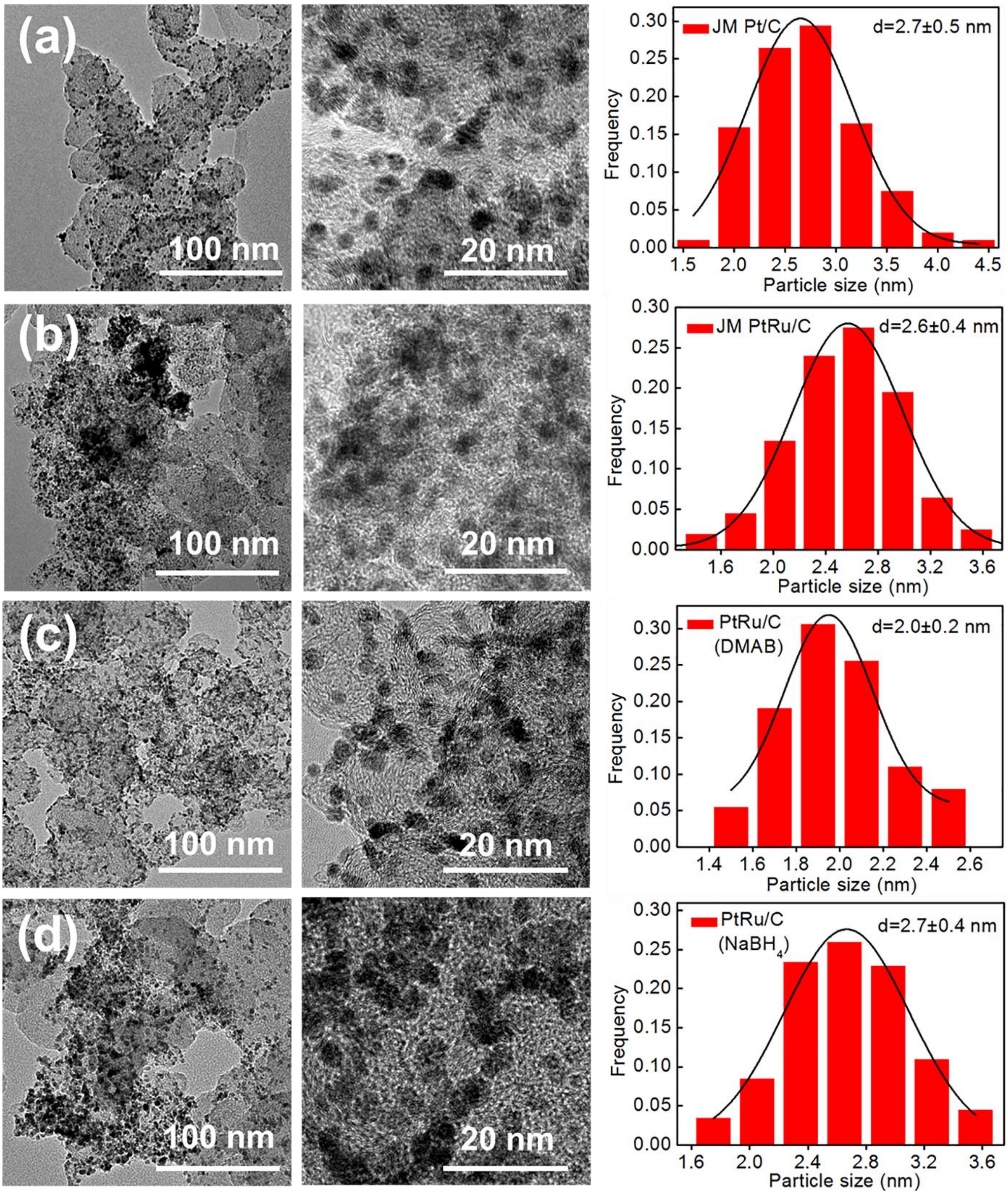

Figure 1. TEM images and corresponding particle size distribution histograms of (**a**) JM Pt/C, (**b**) JM PtRu/C, (**c**) PtRu/C(DMAB) and (**d**) PtRu/C($NaBH_4$).

The average metallic particle sizes ($\bar{d}_{XRD}$) for the above catalysts were also calculated from the (111) diffraction peak by applying the Scherrer's equation [36]:

$$d_{XRD} = K\,\lambda\;/\;B\;\cos\theta \tag{7}$$

where K = 0.9 is a constant, λ is the wavelength of a Cu target X-ray (0.154 nm), B is the width of (111) a peak at half height, and θ is the diffraction angle at the maximum of (111) the peak. As shown in Table S1, the average particle sizes thus calculated are in accordance with those characterized by TEM, suggesting uniform size and good crystallinity of these catalysts.

Assuming that the lattice parameters on Ru content for unsupported and carbon-supported Pt-Ru alloys were of the same dependence [37], the alloying degree was semi-quantitatively evaluated by Vegard's law. The lattice parameter (a) values for PtRu/C catalysts may be calculated by using (111) diffraction peaks [38]:

$$a = \sqrt{3}\,\lambda \;/\; 2\,\sin\theta \tag{8}$$

while the alloying degree of PtRu/C (X_{Ru}) may be estimated from the following equation [37]:

$$X_{Ru} = \left(a^0 - a\right) / \,k \tag{9}$$

where a^0 = 0.3916 nm is the lattice parameter for pure Pt/C and k = 0.0124 nm is a constant. The values of a for JM PtRu/C, PtRu/C(DMAB) and PtRu/C($NaBH_4$) are estimated to be 0.3848, 0.3848 and 0.3852 nm, respectively, yielding X_{Ru} values of 55%, 55% and 52% for the three catalysts. The X_{Ru} value for PtRu/C(DMAB) equals to that for JM PtRu/C but is slightly larger than that for PtRu/C($NaBH_4$), as a result of using the milder reductant DMAB.

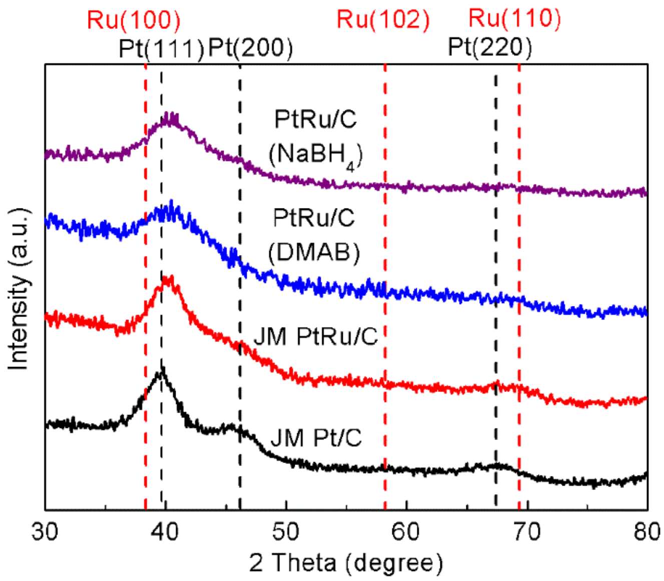

Figure 2. XRD patterns of JM Pt/C, JM PtRu/C, PtRu/C(DMAB) and PtRu/C($NaBH_4$).

The chemical oxidation states and electronic properties were determined by core level XPS spectra. Figure 3a shows the Pt core level XPS spectra of JM Pt/C and PtRu/C catalysts. By deconvoluting the Pt $4f_{7/2}$ and Pt $4f_{5/2}$ doublets, the presence of Pt^0, Pt^{2+} and Pt^{4+} components can be revealed. As listed in Table S2, the Pt^0 $4f_{7/2}$ binding energies equal to 71.1, 71.4, 72.3 and 72.0 eV for JM Pt/C, JM PtRu/C, PtRu/C(DMAB) and PtRu/C($NaBH_4$), respectively. Specifically, the positive shift can be attributed to the partial electron transfer from Ru to Pt which lowers the d-band center of Pt sites or weakens the adsorption of CO intermediate on PtRu/C(DMAB) [12]. What's more, as seen from Figure 3b and Table S3, the relative peak intensity for Ru^0 to Ru(IV) on PtRu/C(DMAB) is larger than that on JM PtRu/C or PtRu/C($NaBH_4$). The metallic Ru rather than the RuO_2 was actually suggested to contribute to the bifunctional mechanism [39,40], providing sufficient Ru-OH to accelerate the oxidation of Pt-CO on PtRu/C(DMAB).

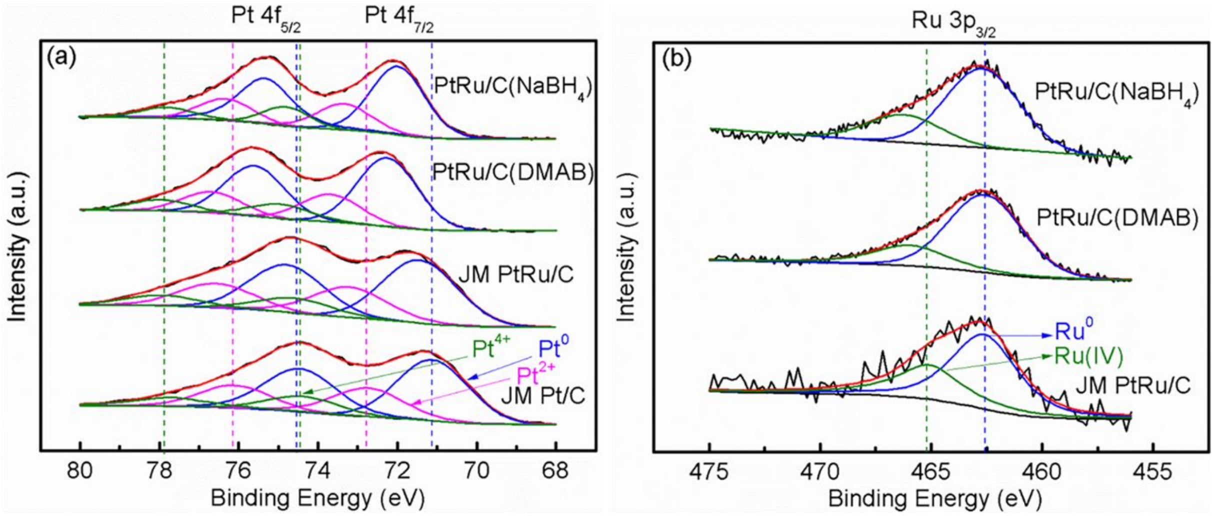

Figure 3. Regional core level XPS spectra of (**a**) Pt 4f and (**b**) Ru $3p_{3/2}$ for JM Pt/C, JM PtRu/C, PtRu/C(DMAB) and PtRu/C($NaBH_4$) catalysts.

2.3. Electrochemical Performance

In Figure 4a, cyclic voltammograms (CVs) of JM Pt/C and PtRu/C catalysts in 0.5 M H_2SO_4 present electrochemical voltametric features typical of Pt and PtRu electrodes. No distinct hydrogen adsorption/desorption peaks except larger double-layer currents can be observed on PtRu/C catalysts, compared to the corresponding counterparts on JM Pt/C. The electrochemical surface areas (ECSAs) of these catalysts may be evaluated by means of the anodic CO stripping shown in Figure 4b, according to the following equation,

$$\text{ECSA} = Q / (m \times v \times Q_{\text{CO}}) \tag{10}$$

where Q is the integrated charge of the CO ad-layer, m is the total mass of Pt loaded on GCE, v is the scan rate and Q_{CO} is ca. 0.42 mC cm^{-2} for the oxidation of CO monolayer. Specifically, the previous ATR-IR studies showed that the relative CO amount on Ru sites of a PtRu alloy was very small [41,42]. As a result, the ECSAs can be normalized to the Pt mass, which are estimated to be 85.8, 94.3, 126.3 and 141.9 $m^2 \cdot g^{-1}\ _{\text{Pt}}$ for JM Pt/C, JM PtRu/C, PtRu/C($NaBH_4$) and PtRu/C(DMAB), respectively. Besides, as detailed in Table S4, the onset and peak potentials of oxidative CO removal on PtRu/C(DMAB) are shifted by ca. −280 mV as compared to those on JM Pt/C, and present a slightly negative shift relative to those on JM PtRu/C and PtRu/C($NaBH_4$), indicating the weakest CO adsorption on PtRu/C(DMAB), which is concomitant with the XPS characterizations. The better CO resistance and larger ECSA of PtRu/C(DMAB) are expected to be consistent with its higher MOR activity and durability.

The methanol electro-oxidation activities of JM Pt/C, JM PtRu/C, PtRu/C(DMAB) and PtRu/C($NaBH_4$) catalysts were also compared by CVs. Figure 5a depicts Pt-mass normalized CVs for Pt-based catalysts in 0.5 M H_2SO_4 containing 1 M CH_3OH solution at 50 mV s^{-1}. It can be seen that PtRu/C(DMAB) exhibits a higher peak current density of 0.53 A $mg^{-1}\ _{\text{Pt}}$, which is about 1.5 and 1.8 times of those obtained on JM Pt/C (0.36 A $mg^{-1}\ _{\text{Pt}}$) and JM PtRu/C (0.30 A $mg^{-1}\ _{\text{Pt}}$), respectively. Besides, as shown in Table S5, the ratio between the forward (i_f) and backward peak current density (i_b) on PtRu/C(DMAB) is comparable to that on JM PtRu/C but is higher than the counterparts on JM Pt/C and PtRu/C($NaBH_4$). A higher i_f / i_b ratio was previously used as a criterion for CO tolerance [43–46], and more recently as an indicator of a more oxyphilic surface or enhanced OH formation [47,48], in favor of MOR to CO_2 conversion at lower potentials in the preceding forward scan. The MOR parameters of the PtRu/C catalysts from this work and recent publications are listed in Table S6 for comparison. Notably, the peak potential of CO oxidation on PtRu/C(DMAB) is 0.252 V (vs. SCE), which is more negative than those reported in the literature, in favor of the MOR to CO_2 conversion at lower potentials. The better CO tolerance and higher mass activity of the PtRu/C(DMAB) together with the aqueous synthesis benefits the scaled-up application of this catalyst.

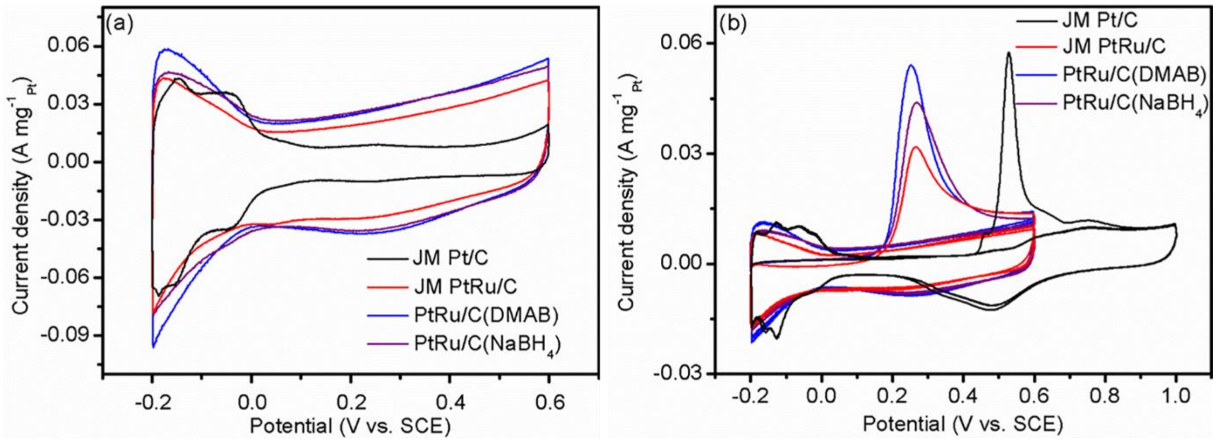

Figure 4. Pt-mass normalized (**a**) cyclic and (**b**) CO stripping voltammograms on JM Pt/C, JM PtRu/C, PtRu/C(DMAB) and PtRu/C($NaBH_4$) catalysts in 0.5 M H_2SO_4, at a scan rate of 50 (left panel) and 10 (right panel) mV s^{-1}.

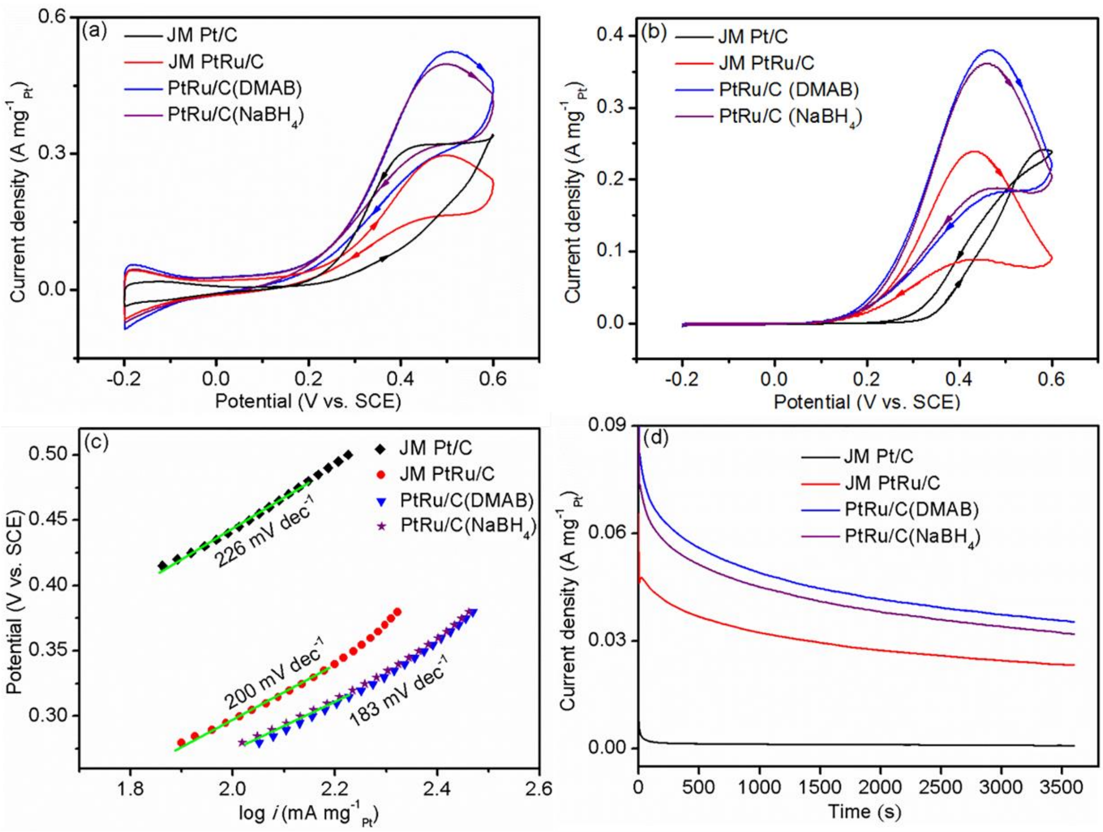

Figure 5. Electro-oxidation performance on JM Pt/C, JM PtRu/C, PtRu/C(DMAB) and PtRu/C($NaBH_4$) catalysts: (**a**,**b**) Pt-mass normalized CVs at a scan rate of (**a**) 50 mV s^{-1} and (**b**) 1 mV s^{-1}; (**c**) the Tafel plots redrawn from (**b**); (**d**) Chronoamperometry curves at a constant potential of 0.25 V in 0.5 M H_2SO_4 + 1 M CH_3OH.

Figure 5b shows the CVs in 0.5 M H_2SO_4 containing 1 M CH_3OH solution at 1 mV s^{-1} to mimic a quasi-steady-state measurement. The corresponding Tafel plots in Figure 5c shows the apparent Tafel slopes for the PtRu/C(DMAB) and PtRu/C ($NaBH_4$) are both ca. 183 mV dec^{-1}, close to that obtained for the commercial PtRu/C (200 mV dec^{-1}) and appreciably lower than that for the commercial Pt/C (226 mV dec^{-1}). The smaller apparent

Tafel slope on the PtRu/C(DMAB) together with the larger oxidation peak current suggests that the DMAB-derived PtRu/C catalyst at least demonstrates a higher activity in a half cell measurement condition, thus deserving of a further test as the real anode catalyst in a single direct methanol fuel cell.

In order to further evaluate the long-time stability, chronoamperometric curves were recorded at a practical potential of 0.25 V. As shown in Figure 5d, PtRu/C(DMAB) exhibits a current density of 35.4 mA mg^{-1} $_{Pt}$ for 1 h electrooxidation, which is 44, 1.52 and 1.11 times as high as that obtained on JM Pt/C (0.8 mA mg^{-1} $_{Pt}$), JM PtRu/C (23.3 mA mg^{-1} $_{Pt}$) and PtRu/C($NaBH_4$) (31.9 mA mg^{-1} $_{Pt}$), respectively. Again, the enhanced MOR performance on PtRu/C(DMAB) is consistent with the structural characterization results.

2.4. Preliminary DMFC Test

The electrical characteristics of the DMFCs incorporating the above anode catalysts were measured to evaluate their potential application. Figure 6 compares the plots of the output voltage and power density versus current density of the DMFCs fed with 1 M methanol at 80 °C at a given Pt mass loading. The highest current density of the DMFC with PtRu/C(DMAB) is 464 mA cm^{-2}, which is higher than that of JM Pt/C (200 mA cm^{-2}), PtRu/C($NaBH_4$) (400 mA cm^{-2}) or JM PtRu/C (439 mA cm^{-2}). In terms of peak power density, the DMFC with JM Pt/C yields the lowest value (41.1 mW cm^{-2}), and the one with PtRu/C(DMAB) gives the highest one (96.3 mW cm^{-2}). The latter is ca. 18% and 9% higher than that with PtRu/C($NaBH_4$) (81.8 mW cm^{-2}) and the state-of-the-art JM PtRu/C (88.7 mW cm^{-2}), respectively, in harmony with the electrochemical measurements. What's more, we understand that the fuel cell performance relies heavily on the membrane electrode assembly (MEA) preparation technology besides the catalysts [28,49,50], optimizing the microstructures of MEA in the near future could lead to an upgraded output performance of the DMFC with the PtRu/C(DMAB). By the way, the JM PtRu/C is speculated as a sosoloid by considering its poor solubility in a hot aqua regia, for which structure special post heat-treatment is often required following the organic phase synthesis of a catalyst. In this regard, our facile aqueous phase synthesis of the PtRu/C(DMAB) provides an alternate solution to the anode catalyst of DMFCs.

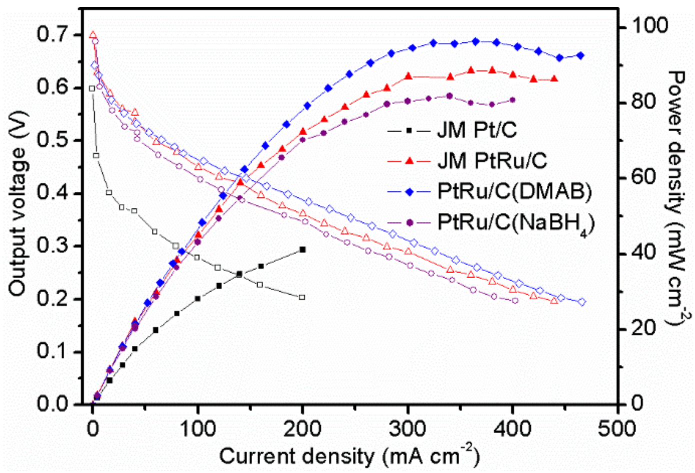

Figure 6. The electrical performance of DMFCs with an anode catalyst of JM Pt/C, JM PtRu/C, PtRu/C(DMAB) and PtRu/C($NaBH_4$), respectively, all with the 60 wt.% JM Pt/C cathode catalyst. 1 M methanol was fed in, and the working temperature was set to 80 °C. The right column and solid symbols represent the power density vs. current density curves while the left column and hollow symbols represent the output voltage vs. current density curves.

2.5. Interfacial Species Evolved during MOR

In-situ ATR-IR spectroscopy was employed to trace the evolution of adsorbed intermediates and dissolved products of methanol dissociation and oxidation while the potential was scanned positively. The spectral results are shown in Figure 7 and the detailed band assignments are summarized in Table S7. Briefly, in Figure 7a–c, the strong band at 2019~2053 cm^{-1} can be assigned to the linearly bonded CO on Pt (Pt-CO_L), and the weak bands at 1935~1972 cm^{-1} belong to the Ru-CO_L due to methanol dehydrogenation, together with the band at ~1610 cm^{-1} due to the δ(HOH) of interfacial water. The downward IR bands at ~1723 and ~1323 cm^{-1} can be assigned to dissolved formic acid (HCOOH) and bridge-bonded fomite ($HCOO_B$), respectively, given that the reference spectrum is taken at 1.0 V. These observed results are consistent with the so-called dual reaction pathways for MOR, i.e., the CO-pathway and the non-CO (via fomite-formic acid) pathway [51–53]. The normalized CO_L band intensities as a function of potential are plotted in Figure 8. The CO_L bands on JM Pt/C, PtRu/C and PtRu/C(DMAB) decrease by ca. 35%, 50%, and 60%, respectively, as the potential increases from 0.1 V to 0.6 V. The more rapid drop of the CO_L band with increasing potential, or the higher CO-resistance arises from the bifunctional mechanism on PtRu alloys [54]. The CO_2 produced during MOR was detected with the asymmetric stretch band at ~2340 cm^{-1}, as shown in Figure 7d. The normalized CO_2 band intensities versus potential are compared in Figure 8 for the three corresponding catalysts. It can be seen that the CO_2 band on the PtRu/C(DMAB) shows up at the most negative potential, as its band intensity reaches 100%, indicating that it is the most promoted 6-electron MOR on this home-synthesized catalyst. Thus, the ATR-IR results further prove the enhanced electrocatalytic and DMFC performance of the as-synthesized PtRu/C(DMAB) at a molecular level.

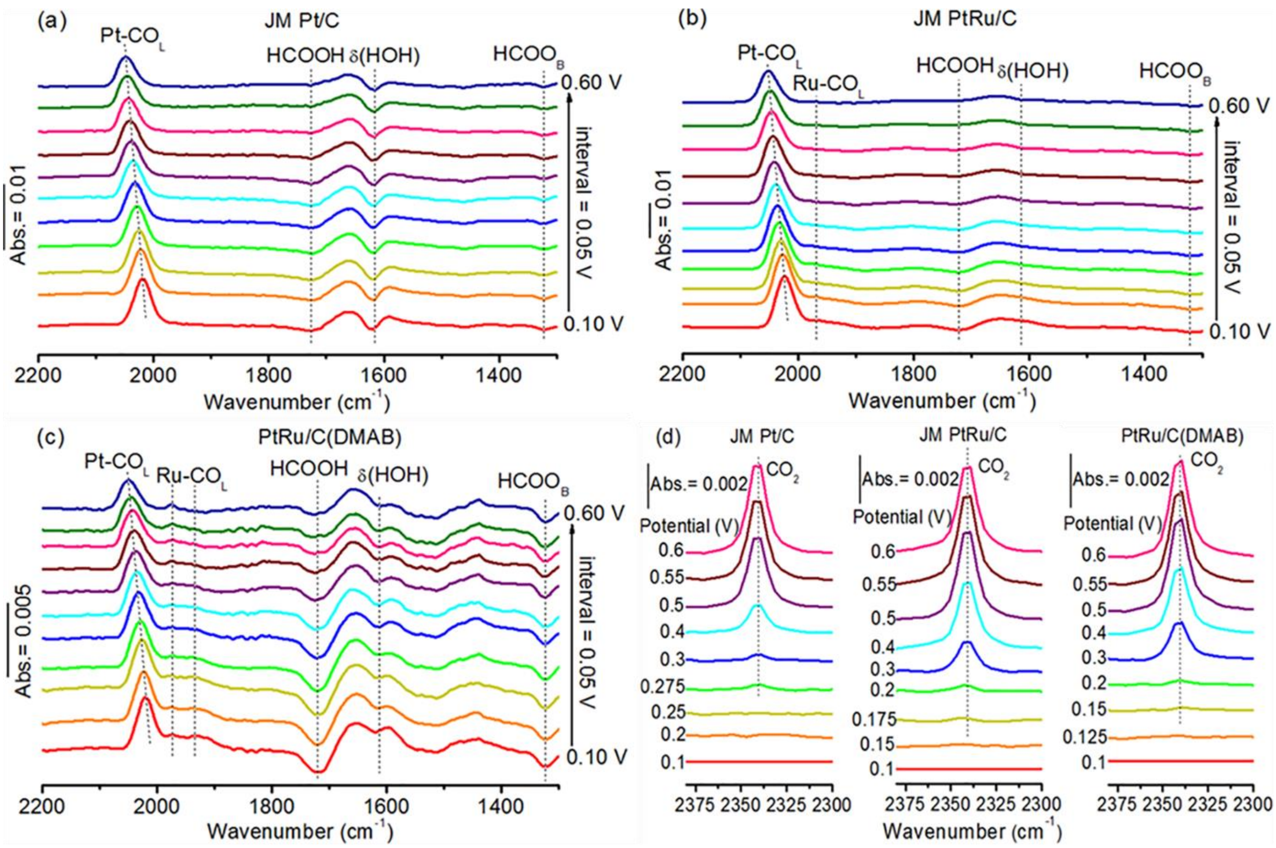

Figure 7. The potential dynamic ATR-IR spectra for the electro-oxidation on JM Pt/C, JM PtRu/C and PtRu/C(DMAB) in 0.5 M H_2SO_4 and 1 M CH_3OH, at a scan rate of 5 mV s^{-1}. Reference spectrum is taken at (**a**–**c**) 1.0 V (vs. SCE) or (**d**) 0.1 V (vs. SCE).

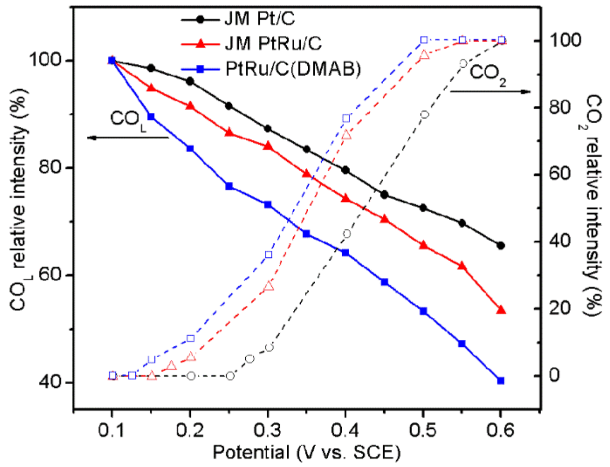

Figure 8. Potential-dependent CO_L (left column, solid lines and solid symbols) and CO_2 (right column, dashed lines and hollow symbols) relative intensities for JM Pt/C, JM PtRu/C and PtRu/C(DMAB).

3. Materials and Methods

3.1. Reagents

Trisodium citrate dihydrate ($Na_3C_6H_5O_7{\cdot}2H_2O$, A.R.), ruthenium trichloride ($RuCl_3$, G.R.), potassium chloroplatinate (K_2PtCl_4, A.R.), hydrochloric acid (HCl, A.R.) and sodium borohydride ($NaBH_4$, A.R.) were all purchased from Sinopharm Chemical Reagent Company (Shanghai, China). Vulcan XC-72 carbon black and DMAB were obtained from Cabot (Boston, MA, USA) and Aladdin (Shanghai, China), respectively. Commercial Pt/C and PtRu/C catalysts with a 20 wt.% Pt metal loading were purchased from the Johnson Matthey Company (London, GLA, UK) and Shanghai Hesen Electrical Company (Shanghai, China), respectively. All of the aqueous solutions were prepared with 18.2 MΩ·cm Milli-Q water (Millipore, Boston, MA, USA), specifically for the precursor salt solution, an additional 1 vol.% HCl was added.

3.2. Preparation of Catalysts

The PtRu/C(DMAB) was prepared by a so-called reverse addition of aqueous phase synthesis. Briefly, in a 100 mL three-necked bottle, 56 mg of refluxed Vulcan XC-72 carbon black was added to 20 mL of Milli-Q water. The slurry was sonicated for 45 min, and stirred at 750 rpm for 1 h in an ice-water bath with a N_2-bubbled atmosphere. Then, 250 mg of $Na_3C_6H_5O_7{\cdot}2H_2O$ and 294.6 mg of DMAB were added into the slurry, which was further stirred to ensure the complete dissolution of the two chemicals. Next, 10 mL of aqueous solution (to suppress the hydrolysis of the metallic precursors, additional 1 vol.% HCl was added) containing 34 mg of K_2PtCl_4 and 17 mg of $RuCl_3$ was added dropwise to the suspension via a peristaltic pump at 1 mL min^{-1}. The suspension was kept stirring at 900 rpm in an ice-water bath and a N_2-bubbled atmosphere for another 4 h. After that, the slurry was stirred at 30 °C overnight to ensure the complete decomposition of the remaining DMAB. The powder was thereafter filtered out of the suspension, and rinsed with 5 mL of 0.1 mol L^{-1} CH_3COOH and copious amount of ultrapure water, respectively. The as-prepared PtRu/C(DMAB) was dried in a vacuum oven at 80 °C for 8 h. The PtRu/C($NaBH_4$) catalyst was prepared according to the otherwise same procedures except that 189.2 mg of $NaBH_4$ was used as the reducing agent instead of DMAB.

For comparison, the PtRu/C(DMAB) and PtRu/C($NaBH_4$) catalysts were also prepared by a regular addition of aqueous phase synthesis, namely, one of the reductants was added dropwise into the aqueous solution containing carbon black and Pt(II)-Ru(III) precursors with otherwise the same conditions as described above.

3.3. Material Characterization

The compositions of the catalysts were determined by inductively coupled plasma-atomic emission spectroscopy (ICP-AES, Thermo Fisher iCAP 7400, Thermo Fisher China, Shanghai, China). The crystalline phase structures of the nanoparticles were examined by X-ray diffraction (XRD, Bruker D8 Discovery A25, Bruker AXS, Karlruher, BW, Germany) with the Cu $K\alpha$ radiation at the 2θ angle from 30° to 80°. The morphology and size distributions of the catalysts were characterized by transmission electron microscope (TEM, FEI Tecnai G2 F20 S-Twin, FEI, Hillsboro, OR, USA). The metallic electronic structures were analyzed by X-ray photoelectron spectroscopy (XPS, PHI 5000C&PHI 5300, PHI, Lafayette, LA, USA) with Mg $K\alpha$ radiation and the C 1s peak at 284.6 eV was used for calibrating the binding energies.

3.4. Electrochemical Measurements

The working electrode was a glassy carbon electrode (GCE, 3 mm in diameter) coated with different catalyst layers. A saturated calomel electrode (SCE) and a Pt gauze were used as the reference and counter electrodes, respectively, in a three-compartment cell. An electrochemical workstation (Model 605B, CH Instruments, Shanghai, China) was used to control potential and measure current with an 80% iR drop compensation. All electrochemical measurements were run at 25 ± 1 °C.

First, 2 mg of the catalysts, 800 μL of Milli-Q water, 200 μL of isopropanol and 20 μL of 5 wt.% Nafion were mixed and sonicated to form a uniform catalyst ink, then 5.1 μL of the ink was coated onto a polished GCE via a micropipette and dried with the aid of infrared radiation. The Pt loading was set to be 28 μg cm^{-2} on each working electrode. Cyclic voltammograms of MOR on different catalysts were measured in 1 M CH_3OH + 0.5 M H_2SO_4 at 50 mV s^{-1}, while chronoamperometric curves were recorded in the same solution at 0.25 V for 3600 s. Prior to the above measurements, the catalysts were subjected to multiple cycles of potential scan in 0.5 M H_2SO_4 to attain clean surfaces. Notably, the upper potential limit was set to be 0.6 V to avoid the oxidative leaching of the Ru component [55,56]. The ECSAs were evaluated by the anodic CO stripping voltammetry at 10 mV s^{-1} in which the tested catalysts were predosed in CO-saturated solution at 0.05 V followed by N_2-purging.

3.5. Fuel Cell Performance Test

In the single cell test, the MEA was a catalyst coated membrane electrode prepared by ultrasonic spraying. Further, 20 wt.% Pt/C or 30 wt.% PtRu/C was employed as the anode catalyst, with a Pt loading of 0.8 mg cm^{-2}, and 60 wt.% JM Pt/C was used as the cathode catalyst, with a Pt loading of 2 mg cm^{-2}. The cathode and anode catalysts were sprayed onto one and the other sides of a Nafion membrane, respectively. The MEA output performance was assessed at 80 °C by feeding 1 M methanol at a flow rate of 35 mL min^{-1} and pure oxygen at a flow rate of 0.3 slpm (standard liters per minute).

3.6. In-Situ ATR-IR Measurement

The in-situ ATR-IR measurement was run on a Nicolet iS50 IR spectrometer (Thermo Fisher Scientific, Waltham, MA, USA) with a built-in MCT-A detector at an incidence angle of ca. 60° in conjunction with the electrochemical workstation. The working electrode was a catalyst layer coated on an Au electroless under-film pre-deposited on the reflecting plane of a hemicylindrical Si prism, as detailed in our previous reports [51,57,58]. A graphite rod and an SCE served the counter and reference electrodes, respectively. The catalyst ink was prepared by sonicating a mixture of 5 mg of the catalysts, 1 mL of isopropanol and 50 μL of 5 wt.% Nafion, then 105 μL of the ink was pipetted on the IR window and dried to attain a Pt loading of 127 μg cm^{-2}. The resulting ATR-IR spectra were calculated according to A = –lg(R_s / R_r), where R_s and R_r represented the reflected single-beam intensities obtained at the sample and reference potentials, respectively.

4. Conclusions

In summary, we have initially reported a simple, cost-effective and facile DMAB-based aqueous phase approach to synthesize the PtRu/C(DMAB) with a desired 1:1 stoichiometric ratio. PtRu nanoparticles are well-dispersed on carbon support in the PtRu/C(DMAB) with mean particle sizes being smaller than those in the PtRu/C($NaBH_4$) or the commercial PtRu/C, concomitant with the most enhanced CO tolerance and MOR activity. What's more, in-situ ATR-IR spectroscopy further corroborates the electrocatalytic performance at a molecular level. The higher power density of a DMFC with the PtRu/C(DMAB) anode catalyst together with the facile aqueous synthesis of this catalyst paves the way for its potential scaled-up application.

Supplementary Materials: The following are available online at https://www.mdpi.com/article/10.3390/catal11080925/s1, Table S1: The average particle sizes of JM Pt/C, JM PtRu/C, PtRu/C(DMAB) and PtRu/C($NaBH_4$) catalysts obtained from XRD and TEM (simply named as $\overline{d}_{XRD}$ and $\overline{d}_{TEM}$), respectively; Table S2: The binding energies and relative intensities of Pt^0 $4f_{7/2}$ core level XPS spectra for JM Pt/C, JM PtRu/C, PtRu/C(DMAB) and PtRu/C($NaBH_4$) catalysts; Table S3: The binding energies and relative intensities of Ru^0 $3p_{3/2}$ core level XPS spectra for JM PtRu/C, PtRu/C(DMAB) and PtRu/C($NaBH_4$) catalysts; Table S4: The onset (E_{onset}) and peak potentials (E_{peak}) of CO stripping on JM Pt/C, JM PtRu/C, PtRu/C(DMAB) and PtRu/C($NaBH_4$) catalysts in 0.5 M H_2SO_4; Table S5: The electro-oxidation performance on JM Pt/C, JM PtRu/C, PtRu/C(DMAB) and PtRu/C($NaBH_4$) catalysts in 0.5 M H_2SO_4 + 1 M CH_3OH at a scan rate of 50 mV/s (columns 2–4) or a constant potential of 0.25 V (column 5); Table S6: Comparison of synthetic process, particle size and MOR parameters of the PtRu/C catalysts from this work and recent publications; Table S7: IR band assignments in this work.

Author Contributions: Investigation, material synthesis and characterization, electrochemical measurements, writing original draft, Q.W.; investigation, In-situ ATR-IR measurement, Y.-W.Z.; conducting DMFC test, Z.J.; literature survey and counseling, C.C., H.L.; conceptualization, Supervision, project administration, writing—review & editing, W.-B.C. All authors have read and agreed to the published version of the manuscript.

Funding: This work was supported by the National Natural Science Foundation of China (NSFC) (21733004), the International Cooperation Program of Shanghai Science and Technology Committee (STCSM) (17520711200), the National Basic Research Program of China (973 Program, 2015CB932303) and Shanghai Science and Technology Committee (19DZ2270100).

Data Availability Statement: The data presented in this study are available in the manuscript (Table 1, Figures 1–8) and supplementary materials (Tables S1–S7).

Acknowledgments: We highly appreciate Junjie Ge and Wei Xing at Changchun Institute of Applied Chemistry, Chinese Academy of Sciences for kindly arranging the DMFC test.

Conflicts of Interest: The authors declare no conflict of interest.

References

1. Gong, L.; Yang, Z.; Li, K.; Xing, W.; Liu, C.; Ge, J. Recent Development of Methanol Electrooxidation Catalysts for Direct Methanol Fuel Cell. *J. Energy Chem.* **2018**, *27*, 1618–1628. [CrossRef]
2. Yang, Z.; Shi, Y.; Wang, X.; Zhang, G.; Cui, P. Boron as a Superior Activator for Pt Anode Catalyst in Direct Alcohol Fuel Cell. *J. Power Sources* **2019**, *431*, 125–134. [CrossRef]
3. Zhou, Z.-Y.; Shang, S.-J.; Tian, N.; Wu, B.-H.; Zheng, N.-F.; Xu, B.-B.; Chen, C.; Wang, H.-H.; Xiang, D.-M.; Sun, S.-G. Shape Transformation from Pt Nanocubes to Tetrahexahedra with Size near 10 nm. *Electrochem. Commun.* **2012**, *22*, 61–64. [CrossRef]
4. Chen, J.; Luo, S.; Liu, Y.; Chen, S. Theoretical Analysis of Electrochemical Formation and Phase Transition of Oxygenated Adsorbates on Pt(111). *ACS Appl. Mater. Interfaces* **2016**, *8*, 20448–20458. [CrossRef]
5. Zhang, L.; Zhang, X.-F.; Chen, X.-L.; Wang, A.-J.; Han, D.-M.; Wang, Z.-G.; Feng, J.-J. Facile Solvothermal Synthesis of $Pt_{71}Co_{29}$ Lamellar Nanoflowers as an Efficient Catalyst for Oxygen Reduction and Methanol Oxidation Reactions. *J. Colloid Interface Sci.* **2019**, *536*, 556–562. [CrossRef]
6. Zhao, H.; Qi, W.; Zhou, X.; Wu, H.; Li, Y. Composition-controlled Synthesis of Platinum and Palladium Nanoalloys as Highly Active Electrocatalysts for Methanol Oxidation. *Chin. J. Catal.* **2018**, *39*, 342–349. [CrossRef]
7. Liu, H.; Song, C.; Zhang, L.; Zhang, J.; Wang, H.; Wilkinson, D.P. A Review of Anode Catalysis in the Direct Methanol Fuel Cell. *J. Power Sources* **2006**, *155*, 95–110. [CrossRef]

8. Watanabe, M.; Motoo, S. Electrocatalysis by Ad-atoms.2. Enhancement of Oxidation of Methanol on Platinum by Ruthenium Ad-atoms. *J. Electroanal. Chem.* **1975**, *60*, 267–273. [CrossRef]
9. Demirci, U.B. Theoretical Means for Searching Bimetallic Alloys as Anode Electrocatalysts for Direct Liquid-feed Fuel Cells. *J. Power Sources* **2007**, *173*, 11–18. [CrossRef]
10. Liu, J.; Jiang, L. Electrostatic Self-assembly of Pt Nanoparticles on Hexagonal Tungsten Oxide as an Active CO-tolerant Hydrogen Oxidation Electrocatalyst. *Int. J. Hydrog. Energy* **2018**, *43*, 8944–8952. [CrossRef]
11. Wang, Z.-B.; Yin, G.-P.; Lin, Y.-G. Synthesis and Characterization of PtRuMo/C Nanoparticle Electrocatalyst for Direct Ethanol Fuel Cell. *J. Power Sources* **2007**, *170*, 242–250. [CrossRef]
12. Wakisaka, M.; Mitsui, S.; Hirose, Y.; Kawashima, K.; Uchida, H.; Watanabe, M. Electronic Structures of Pt-Co and Pt-Ru Alloys for CO-tolerant Anode Catalysts in Polymer Electrolyte Fuel Cells Studied by EC-XPS. *J. Phys. Chem. B* **2006**, *110*, 23489–23496. [CrossRef]
13. Zhang, J.; Qu, X.; Han, Y.; Shen, L.; Yin, S.; Li, G.; Jiang, Y.; Sun, S. Engineering PtRu Bimetallic Nanoparticles with Adjustable Alloying Degree for Methanol Electrooxidation: Enhanced Catalytic Performance. *Appl. Catal. B Environ.* **2020**, *263*, 118345. [CrossRef]
14. Chetty, R.; Kundu, S.; Xia, W.; Bron, M.; Schuhmann, W.; Chirila, V.; Brandl, W.; Reinecke, T.; Muhler, M. PtRu Nanoparticles Supported on Nitrogen-doped Multiwalled Carbon Nanotubes as Catalyst for Methanol Electrooxidation. *Electrochim. Acta* **2009**, *54*, 4208–4215. [CrossRef]
15. Carmo, M.; Paganin, V.A.; Rosolen, J.M.; Gonzalez, E.R. Alternative Supports for the Preparation of Catalysts for Low-temperature Fuel Cells: The Use of Carbon Nanotubes. *J. Power Sources* **2005**, *142*, 169–176. [CrossRef]
16. Takasu, Y.; Fujiwara, T.; Murakami, Y.; Sasaki, K.; Oguri, M.; Asaki, T.; Sugimoto, W. Effect of Structure of Carbon-supported PtRu Electrocatalysts on the Electrochemical Oxidation of Methanol. *J. Electrochem. Soc.* **2000**, *147*, 4421–4427. [CrossRef]
17. Harish, S.; Baranton, S.; Coutanceau, C.; Joseph, J. Microwave Assisted Polyol Method for the Preparation of Pt/C, Ru/C and PtRu/C Nanoparticles and its Application in Electrooxidation of Methanol. *J. Power Sources* **2012**, *214*, 33–39. [CrossRef]
18. Neto, A.O.; Dias, R.R.; Tusi, M.M.; Linardi, M.; Spinacé, E.V. Electro-oxidation of Methanol and Ethanol Using PtRu/C, PtSn/C and PtSnRu/C Electrocatalysts Prepared by an Alcohol-Reduction Process. *J. Power Sources* **2007**, *166*, 87–91. [CrossRef]
19. Liu, Z.; Lee, J.Y.; Han, M.; Chen, W.; Gan, L.M. Synthesis and Characterization of PtRu/C Catalysts from Microemulsions and Emulsions. *J. Mater. Chem.* **2002**, *12*, 2453–2458. [CrossRef]
20. Liu, Z.L.; Ling, X.Y.; Su, X.D.; Lee, J.Y. Carbon-supported Pt and PtRu Nanoparticles as Catalysts for a Direct Methanol Fuel Cell. *J. Phys. Chem. B* **2004**, *108*, 8234–8240. [CrossRef]
21. Bock, C.; Paquet, C.; Couillard, M.; Botton, G.A.; MacDougall, B.R. Size-selected Synthesis of PtRu Nano-catalysts: Reaction and Size Control Mechanism. *J. Am. Chem. Soc.* **2004**, *126*, 8028–8037. [CrossRef]
22. Zhang, X.; Chan, K.Y. Water-in-oil Microemulsion Synthesis of Platinum-Ruthenium Nanoparticles, Their Characterization and Electrocatalytic Properties. *Chem. Mater.* **2003**, *15*, 451–459. [CrossRef]
23. Okaya, K.; Yano, H.; Uchida, H.; Watanabe, M. Control of Particle Size of Pt and Pt Alloy Electrocatalysts Supported on Carbon Black by the Nanocapsule Method. *ACS Appl. Mater. Interfaces* **2010**, *2*, 888–895. [CrossRef]
24. Bang, J.H.; Han, K.; Skrabalak, S.E.; Kim, H.; Suslick, K.S. Porous Carbon Supports Prepared by Ultrasonic Spray Pyrolysis for Direct Methanol Fuel Cell Electrodes. *J. Phys. Chem. C* **2007**, *111*, 10959–10964. [CrossRef]
25. Xue, X.; Lu, T.; Liu, C.; Xing, W. Simple and Controllable Synthesis of Highly Dispersed Pt–Ru/C Catalysts by a Two-step Spray Pyrolysis Process. *Chem. Commun.* **2005**, *12*, 1601–1603. [CrossRef] [PubMed]
26. Silva, J.C.M.; Ntais, S.; Rajaraman, V.; Teixeira-Neto, É.; Teixeira-Neto, Â.A.; Neto, A.O.; Antoniassi, R.M.; Spinacé, E.V.; Baranova, E.A. The Catalytic Activity of Pt:Ru Nanoparticles for Ethylene Glycol and Ethanol Electrooxidation in a Direct Alcohol Fuel Cell. *Electrocatalysis* **2019**, *10*, 203–213. [CrossRef]
27. Guo, J.W.; Zhao, T.S.; Prabhuram, J.; Chen, R.; Wong, C.W. Preparation and Characterization of a PtRu/C Nanocatalyst for Direct Methanol Fuel Cells. *Electrochim. Acta* **2005**, *51*, 754–763. [CrossRef]
28. Montiel, G.; Fuentes-Quezada, E.; Bruno, M.M.; Corti, H.R.; Viva, F.A. Effect of Bimodal Mesoporous Carbon as PtRu Catalyst Support for Direct Methanol Fuel Cells. *RSC Adv.* **2020**, *10*, 30631–30639. [CrossRef]
29. Lizcano-Valbuena, W.H.; Paganin, V.A.; Gonzalez, E.R. Methanol Electro-oxidation on Gas Diffusion Electrodes Prepared with Pt-Ru/C Catalysts. *Electrochim. Acta* **2002**, *47*, 3715–3722. [CrossRef]
30. Ohno, I.; Wakabayashi, O.; Haruyama, S. Anodic-Oxidation of Reductants in Electroless Plating. *J. Electrochem. Soc.* **1985**, *132*, 2323–2330. [CrossRef]
31. Wang, J.-Y.; Kang, Y.-Y.; Yang, H.; Cai, W.-B. Boron-doped Palladium Nanoparticles on Carbon Black as a Superior Catalyst for Formic Acid Electro-oxidation. *J. Phys. Chem. C* **2009**, *113*, 8366–8372. [CrossRef]
32. Dong, Y.; Zhou, Y.-W.; Wang, M.-Z.; Zheng, S.-L.; Jiang, K.; Cai, W.-B. Facile Aqueous Phase Synthesis of Carbon Supported B-doped Pt_3Ni Nanocatalyst for Efficient Oxygen Reduction Reaction. *Electrochim. Acta* **2017**, *246*, 242–250. [CrossRef]
33. Huang, J.; Ding, C.; Yang, Y.; Liu, G.; Cai, W.-B. An Alternate Aqueous Phase Synthesis of the Pt_3Co/C Catalyst towards Efficient Oxygen Reduction Reaction. *Chin. J. Catal.* **2019**, *40*, 1895–1903. [CrossRef]
34. Wang, D.; Zhuang, L.; Lu, J. An Alloying-Degree-Controlling Step in the Impregnation Synthesis of PtRu/C Catalysts. *J. Phys. Chem. C* **2007**, *111*, 16416–16422. [CrossRef]

35. Wang, Q.; Chen, S.; Shi, F.; Chen, K.; Nie, Y.; Wang, Y.; Wu, R.; Li, J.; Zhang, Y.; Ding, W.; et al. Structural Evolution of Solid Pt Nanoparticles to a Hollow PtFe Alloy with a Pt-skin Surface Via Space-confined Pyrolysis and the Nanoscale Kirkendall Effect. *Adv. Mater.* **2016**, *28*, 10673–10678. [CrossRef]
36. Gojković, S.L.; Vidaković, T.R.; Đurović, D.R. Kinetic Study of Methanol Oxidation on Carbon-supported PtRu Electrocatalyst. *Electrochim. Acta* **2003**, *48*, 3607–3614. [CrossRef]
37. Antolini, E.; Cardellini, F. Formation of Carbon Supported PtRu Alloys: An XRD Analysis. *J. Alloys Compd.* **2001**, *315*, 118–122. [CrossRef]
38. Tian, M.; Shi, S.; Shen, Y.; Yin, H. PtRu Alloy Nanoparticles Supported on Nanoporous Gold as an Efficient Anode Catalyst for Direct Methanol Fuel Cell. *Electrochim. Acta* **2019**, *293*, 390–398. [CrossRef]
39. Wang, H.S.; Wingender, C.; Baltruschat, H.; Lopez, M.; Reetz, M.T. Methanol Oxidation on Pt, PtRu, and Colloidal Pt Electrocatalysts: A DEMS Study of Product Formation. *J. Electroanal. Chem.* **2001**, *509*, 163–169. [CrossRef]
40. Parsons, R.; Vandernoot, T. The Oxidation of Small Organic-Molecules—A Survey of Recent Fuel-cell Related Research. *J. Electroanal. Chem.* **1988**, *257*, 9–45. [CrossRef]
41. Sato, T.; Okaya, K.; Kunimatsu, K.; Yano, H.; Watanabe, M.; Uchida, H. Effect of Particle Size and Composition on CO-tolerance at Pt–Ru/C Catalysts Analyzed by in situ Attenuated Total Reflection FTIR Spectroscopy. *ACS Catal.* **2012**, *2*, 450–455. [CrossRef]
42. Watanabe, M.; Sato, T.; Kunimatsu, K.; Uchida, H. Temperature Dependence of CO-adsorption of Carbon Monoxide and Water on Highly Dispersed Pt/C and PtRu/C Electrodes Studied by in-situ ATR-FTIRAS. *Electrochim. Acta* **2008**, *53*, 6928–6937. [CrossRef]
43. Manoharan, R.; Goodenough, J.B. Methanol Oxidation in Acid on Ordered NiTi. *J. Mater. Chem.* **1992**, *2*, 875–887. [CrossRef]
44. Kuai, L.; Wang, S.; Geng, B. Gold–Platinum Yolk–shell Structure: A Facile Galvanic Displacement Synthesis and Highly Active Electrocatalytic Properties for Methanol Oxidation with Super CO-tolerance. *Chem. Commun.* **2011**, *47*, 6093. [CrossRef]
45. Chen, X.; Jiang, Y.; Sun, J.; Jin, C.; Zhang, Z. Highly Active Nanoporous Pt-based Alloy as Anode and Cathode Catalyst for Direct Methanol Fuel Cells. *J. Power Sources* **2014**, *267*, 212–218. [CrossRef]
46. Lee, Y.-W.; Lee, J.-Y.; Kwak, D.-H.; Hwang, E.-T.; Sohn, J.I.; Park, K.-W. Pd@Pt Core–shell Nanostructures for Improved Electrocatalytic Activity in Methanol Oxidation Reaction. *Appl. Catal. B Environ.* **2015**, *179*, 178–184. [CrossRef]
47. Zhao, Y.; Li, X.; Schechter, J.M.; Yang, Y. Revisiting the Oxidation Peak in the Cathodic Scan of the Cyclic Voltammogram of Alcohol Oxidation on Noble Metal Electrodes. *RSC Adv.* **2016**, *6*, 5384–5390. [CrossRef]
48. Chung, D.Y.; Lee, K.-J.; Sung, Y.-E. Methanol Electro-oxidation on the Pt Surface: Revisiting the Cyclic Voltammetry Interpretation. *J. Phys. Chem. C* **2016**, *120*, 9028–9035. [CrossRef]
49. Jing, F.; Sun, R.; Wang, S.; Sun, H.; Sun, G. Effect of the Anode Structure on the Stability of a Direct Methanol Fuel Cell. *Energy Fuels* **2020**, *34*, 3850–3857. [CrossRef]
50. Alias, M.S.; Kamarudin, S.K.; Zainoodin, A.M.; Masdar, M.S. Active Direct Methanol Fuel Cell: An Overview. *Int. J. Hydrogen Energy* **2020**, *45*, 19620–19641. [CrossRef]
51. Zhou, Y.-W.; Chen, Y.-F.; Jiang, K.; Liu, Z.; Mao, Z.-J.; Zhang, W.-Y.; Lin, W.-F.; Cai, W.-B. Probing the Enhanced Methanol Electrooxidation Mechanism on Platinum-Metal Oxide Catalyst. *Appl. Catal. B Environ.* **2021**, *280*, 119393. [CrossRef]
52. Iwasita, T.; Nart, F.C.; Vielstich, W. An FTIR Study of the Catalytic Activity of a 85-15 Pt-Ru Alloy for Methanol Oxidation. *Ber. Bunsen Ges. Phys. Chem* **1990**, *94*, 1030–1034. [CrossRef]
53. Chen, Y.X.; Miki, A.; Ye, S.; Sakai, H.; Osawa, M. Formate, an Active Intermediate for Direct Oxidation of Methanol on Pt Electrode. *J. Am. Chem. Soc.* **2003**, *125*, 3680–3681. [CrossRef] [PubMed]
54. Yajima, T.; Uchida, H.; Watanabe, M. In-situ ATR-FTIR Spectroscopic Study of Electro-oxidation of Methanol and Adsorbed CO at Pt-Ru Alloy. *J. Phys. Chem. B* **2004**, *108*, 2654–2659. [CrossRef]
55. Wang, H.; Jusys, Z.; Behm, R.J. Ethanol Electro-oxidation on Carbon-supported Pt, PtRu and Pt_3Sn Catalysts: A Quantitative DEMS Study. *J. Power Sources* **2006**, *154*, 351–359. [CrossRef]
56. Jusys, Z.; Kaiser, J.; Behm, R.J. Composition and Activity of High Surface Area PtRu Catalysts towards Adsorbed CO and Methanol Electrooxidation—A DEMS Study. *Electrochim. Acta* **2002**, *47*, 3693–3706. [CrossRef]
57. Wang, J.-Y.; Zhang, H.-X.; Jiang, K.; Cai, W.-B. From HCOOH to CO at Pd Electrodes: A Surface-enhanced Infrared Spectroscopy Study. *J. Am. Chem. Soc.* **2011**, *133*, 14876–14879. [CrossRef] [PubMed]
58. Zhang, H.-X.; Wang, S.-H.; Jiang, K.; André, T.; Cai, W.-B. In situ Spectroscopic Investigation of CO Accumulation and Poisoning on Pd Black Surfaces in Concentrated HCOOH. *J. Power Sources* **2012**, *199*, 165–169. [CrossRef]